

August 2007

Comparative dynamics of magnetically, acoustically, and Brownian motion driven microcantilevers in liquids

Xin Xu

Purdue University, xin@purdue.edu

Arvind Raman

Birck Nanotechnology Center, Purdue University, raman@purdue.edu

Follow this and additional works at: <http://docs.lib.purdue.edu/nanopub>

Xu, Xin and Raman, Arvind, "Comparative dynamics of magnetically, acoustically, and Brownian motion driven microcantilevers in liquids" (2007). *Birck and NCN Publications*. Paper 296.
<http://docs.lib.purdue.edu/nanopub/296>

This document has been made available through Purdue e-Pubs, a service of the Purdue University Libraries. Please contact epubs@purdue.edu for additional information.

Comparative dynamics of magnetically, acoustically, and Brownian motion driven microcantilevers in liquids

Xin Xu and Arvind Raman^{a)}

School of Mechanical Engineering and the Birck Nanotechnology Center, Purdue University, West Lafayette, Indiana 47907

(Received 12 May 2007; accepted 19 June 2007; published online 7 August 2007)

Magnetic, acoustic, and thermal (Brownian motion induced) excitations are commonly used for dynamic atomic force microscopy (AFM) in liquids, yet the fundamental differences in microcantilever vibration response for these different excitations remain poorly understood. In this work we discuss theoretically and experimentally several major differences between the amplitude and phase response of magnetically, acoustically, and thermally excited cantilevers in liquids and propose a way to estimate quantitatively the unsteady structure-borne and fluid-borne excitation forces acting on the acoustically excited AFM cantilever. The results have significant implications both for amplitude and frequency modulated AFM operation in liquids. © 2007 American Institute of Physics. [DOI: 10.1063/1.2767202]

I. INTRODUCTION

Dynamic AFM has become a powerful tool for the nanoscale imaging and spectroscopy of biological samples under conditions close to their native environments.^{1,2} In dynamic atomic force microscopy^{3,4} (AFM) a micromechanical cantilever with a sharp nanoscale tip is driven near resonance and scanned over the sample with certain feedback control laws. The amplitude and phase of tip oscillation are then used to extract information about the topography surface properties. Because the lateral forces applied to the sample are very small in dynamic AFM the tip is unlikely to detach weakly bonded samples from the substrate surface.

Magnetic, acoustic, and thermal excitations are the three main ways to oscillate the AFM cantilevers in liquid environments. In the acoustic mode the cantilever is excited by high frequency vibration from a piezoelectric transducer, also known as a dither piezo, attached to the cantilever chip holder. The vibration of the large surface area of the cantilever chip drives unsteady liquid motion in the liquid cell. Thus the cantilever is not only driven by direct inertial excitation due to its oscillating base (the AFM cantilever chip), but also indirectly by the unsteady fluid motion. Thus the cantilever is excited simultaneously by two mechanisms—(a) structure-borne excitation and (b) fluid-borne excitation. For this reason, in a frequency sweep, the measured cantilever response shows spurious resonances due to hydrodynamic modes of the surrounding fluid, the cantilever chip holder and some other parts of the AFM hardware, causing selection of natural frequency of the cantilever difficult.^{3–8} These unwanted mechanical excitations could also disturb the optical path of the detection system, rendering it less sensitive to the approach of sample.⁴ Another problem is that acoustic excitation may result in sonication of molecular samples, causing sample instability and motion.⁹ While it is possible to reduce the spurious resonances by improving the cantilever holder design (Maali *et al.*^{10,11}), it is usually diffi-

cult to eliminate them entirely. Moreover, as we will show in this article, the measured quantity is the bending of the cantilever and not the absolute tip motion. In spite of these potential disadvantages, the acoustic mode is used by accomplished experimental groups to obtain high quality images in liquids; for example, Moreno-Herrero *et al.* successfully imaged purple membranes in liquid, with a relatively high scan speed of 3–7 lines per second.¹ Moreover, frequency modulation AFM (FM-AFM) using acoustic excitation has been developed to achieve true atomic resolution in liquids.^{12,13}

In the magnetic mode⁴ a magnetized cantilever is directly excited by an external magnetic field. Cantilevers can be magnetized by gluing a magnetic particle at the edge of the cantilever;^{14–16} but most commercial magnetized cantilevers have a thin magnetic film deposited behind the tip.^{4,9} Magnetic excitation yields a much clearer vibration response peak, and the measured quantity is the absolute motion of the tip. However, this technique has its own drawbacks: (a) It requires additional hardware and the manufacture of magnetized cantilevers is more complex and expensive, (b) the magnetic coating does not only change the stiffness and bending angle of the cantilever, but the magnetic metal ions could also contaminate the sample, and (c) the liquid cell may be heated by the electromagnet.

When the microcantilever is in thermal equilibrium with the surrounding liquid, it is excited by collisions from the Brownian motion of liquid molecules. This thermal excitation of microcantilevers is commonly used to extract the wet resonance frequencies and quality factors (Q factors) of its resonances. More recently a thermally driven frequency modulated AFM technique has been developed.¹⁷

Several other excitation mechanisms are available to excite the microcantilever, however, they are not as commonly used as the three excitation mechanisms described earlier. For example, Rogers *et al.* successfully used a piezoelectric microactuated probe to create a clear, single peak;⁵ Tamayo *et al.* developed the high Q -factor control technique⁶ to significantly amplify the oscillation amplitude of the cantilever

^{a)}Electronic mail: raman@purdue.edu

alone; Bugiun *et al.* oscillated the cantilever by passing an alternating current along it while it is placed in a permanent magnetic field;⁷ and Ratcliff *et al.* took advantage of the temperature-sensitive bending properties of metal-coated silicon nitride cantilevers to induce vibrations in the lever using a modulated laser.¹⁸

Arguably the most important cantilever excitation mechanisms for AFM operation in liquids remain the magnetic, acoustic, and thermal excitations; yet the differences in cantilever dynamics between these three excitations remain poorly understood. Furthermore, in acoustic mode AFM it is not at all clear how the cantilever is actually excited—whether by inertial excitation from a vibrating base (structure-borne excitation) or from unsteady fluid motion generated by the vibrating cantilever chip (fluid-borne excitation). Without quantitative knowledge of the fluid-borne excitation it is difficult to estimate quantitatively or control the tip-sample interaction force and energy dissipation.

In this article, we present careful experiments with several different AFM cantilevers that demonstrate clearly the differences between the amplitude and phase response of the levers due to these different excitations. We also derive simple models based on transfer functions¹⁹ that capture correctly the observed magnetic and thermal excitation response and predict an “ideal” acoustic mode response that does not consider the influence of fluid-borne excitation. Using this ideal theoretical model and the measured response, we propose a simple way to quantify the fluid-borne excitation force acting on the AFM cantilever in the acoustic mode. We show in fact that during acoustic excitation in liquids, the contribution of the fluid-borne excitation is comparable to, sometimes even greater than the structure-borne excitation. Finally, we discuss the implications of our results for dynamic AFM in liquids.

The organization of this article is as follows: in Sec. II we derive the transfer functions for magnetic, ideal acoustic, and Brownian motion driven cantilevers, and propose a way to determine the fluid-borne unsteady hydrodynamic forces in acoustic mode AFM; in Sec. III we set up experiments to verify our theoretical models; and in Sec. IV we discuss the implication of our results for dynamic AFM in liquids and summarize our conclusions.

II. THEORETICAL MODELS AND TRANSFER FUNCTIONS

The measured output from an AFM is the bending (which can be converted to the tip motion relative to the cantilever chip) of the cantilever at its free end, while the inputs can be regarded to be the different forms of excitation. The transfer function of the cantilever in each case is simply the steady state amplitude and phase of the output (cantilever bending) with respect to harmonic input at a specific drive frequency. The development of accurate transfer functions requires (a) accurate modeling of the cantilever dynamics, (b) of the excitation mechanism (input), and (c) of the hydrodynamic resistance of the surrounding fluid which changes significantly the resonance frequency and Q factors of each cantilever mode. In what follows we derive such transfer functions for magnetically, acoustically, and ther-

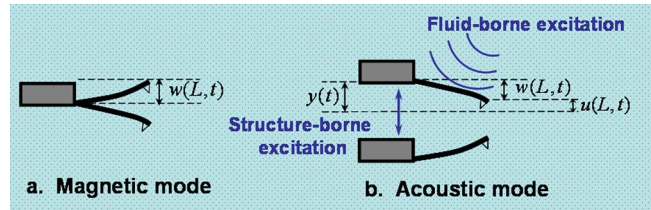


FIG. 1. (Color online) A schematic showing the different tip motions measured in the magnetic mode and acoustic mode. In magnetic mode the measured tip motion is the absolute tip motion $w(x,t)$. While in the acoustic mode the measured motion $w(x,t)$ (transverse cantilever deflection) is the tip motion $u(x,t)$ relative to the base motion $y(t)$.

mally excited cantilevers in fluidic environment. We focus in this article only on the cantilever dynamics in the absence of tip-sample forces. Moreover, we only consider uniform, rectangular levers with the understanding that dynamic response is qualitatively similar regardless of the geometrical shape of the AFM probe.

A. Magnetic mode response

In the magnetic mode the oscillations of the microcantilever about its static equilibrium position [Fig. 1(a)] are governed by

$$EI \frac{\partial^4 w(x,t)}{\partial x^4} + \rho_c A \frac{\partial^2 w(x,t)}{\partial t^2} = f_h(w, \dot{w}) + f_{dr}(t), \quad (1)$$

where $w(x,t)$ is the transverse cantilever deflection, EI is its flexural rigidity, ρ_c is the mass density, L is the length, $A = b \times h$ is the area of the cross section, b and h are the width and thickness of the microcantilever, respectively, f_{dr} is the magnetic excitation force per unit length, and f_h is the hydrodynamic resistance per unit length to cantilever motion. f_h can be derived conveniently for rectangular levers using Tuck–Sader hydrodynamics.^{20–22} Without sample contact, an AFM cantilever is clamped at one end and free at the other end.

We assume that the cantilever is driven near its i th mode resonance frequency. Then the transverse cantilever deflection $w(x,t)$ can be written as

$$w(x,t) = c_i(t) \psi_i(x), \quad (2)$$

where $c_i(t)$ is the complex magnitude of the i th mode, and $\psi_i(x)$ is the normalized eigenfunction of the i th bending mode of a uniform thin rectangular beam.²³ Each eigenfunction is normalized so that $\psi_i(L)=1$, thus $c_i(t)$ is exactly the measured tip motion.

The steady state dynamics of Eq. (1) can be rewritten in the frequency domain using Eq. (2) as

$$EIC_i(\omega) \psi_{i,xxxx}(x) - \omega^2 \rho_c A C_i(\omega) \psi_i(x) = F_h(\omega) + F_{dr}(\omega). \quad (3)$$

For a rectangular cantilever vibrating driven with frequency ω , the hydrodynamic resistance F_h is given by²¹

$$\begin{aligned}
F_h(\omega) &= \frac{\pi}{4} \rho_f b^2 \omega^2 \Gamma_{\text{rect}}(j\omega) W(x|\omega) \\
&= \frac{\pi}{4} \rho_f b^2 \omega^2 \Gamma_{\text{rect}}(j\omega) C_i(\omega) \psi_i(x),
\end{aligned} \quad (4)$$

where ρ_f is the mass density of the surrounding fluid and Γ_{rect} is the hydrodynamic function for a beam with a rectangular cross section. Multiplication of Eq. (3) by $\psi_i(x)$ and integration over the length of the cantilever leads to the following transfer function that is valid for the i th eigenmode of a magnetically excited cantilever

$$\begin{aligned}
\left. \frac{C_i(\omega)}{F_{\text{dr}}(\omega)} \right|_{\text{magnetic}} &= \frac{\beta_i L}{EI(\lambda_i/L)^4 \times \alpha_i L - \omega^2 \left(\rho_c A + \frac{\pi}{4} \rho_f b^2 \Gamma_{\text{rect}} \right) \times \alpha_i L},
\end{aligned} \quad (5)$$

where $\alpha_i L = \int_0^L \psi_i^2 dx$, $\beta_i L = \int_0^L \psi_i dx$, and λ_i is the i th modal wavelength. Note here $F_{\text{dr}}(\omega)$ is the magnetic drive force per unit length. The total magnetic excitation force $F_{\text{dr}}^{\text{total}}(\omega)$ should be $F_{\text{dr}}^{\text{total}}(\omega) = F_{\text{dr}}(\omega) \times L$. For the first mode, $\alpha_1 = 0.2500$, $\beta_1 = 0.3519$, $\lambda_1 = 1.8751$, Eq. (5) becomes

$$\begin{aligned}
\left. \frac{C_1(\omega)}{F_{\text{dr}}^{\text{total}}(\omega)} \right|_{\text{magnetic}} &= \frac{0.3915}{1.0302k_c - \omega^2 \left(\rho_c A + \frac{\pi}{4} \rho_f b^2 \Gamma_{\text{rect}} \right) \times 0.25L},
\end{aligned} \quad (6)$$

where k_c is the cantilever stiffness and $k_c = 3EI/L^3$. Equation (6) gives the transfer function for the first mode of magnetically excited cantilever motion. Given an input magnetic force $F_{\text{dr}}^{\text{total}}(\omega)$, the output, the measured tip motion $C_1(\omega)$, can be calculated using Eq. (6).

B. Ideal acoustic mode response

Figure 1(b) shows the diagram of cantilever motion in acoustic mode in liquids. The cantilever is excited simultaneously by a structure-borne and a fluid-borne excitation. In this section we consider the ideal situation, i.e., we consider only the structure-borne excitation here. In Sec. II E we will include the fluid-borne excitation generated by the vibrating cantilever holder.

The governing equation for the transverse displacements of the cantilever driven in the ideal acoustic mode is

$$EI \frac{\partial^4 u(x,t)}{\partial x^4} + \rho_c A \frac{\partial^2 u(x,t)}{\partial t^2} = f_h(u, \dot{u}), \quad (7)$$

with boundary conditions

$$u(0,t) = y(t), \quad \frac{\partial u(0,t)}{\partial x} = 0,$$

$$\frac{\partial^2 u(L,t)}{\partial x^2} = 0, \quad \frac{\partial^3 u(L,t)}{\partial x^3} = 0, \quad (8)$$

where $u(t)$ is the absolute cantilever motion. As we can see in Fig. 1(b), contrary to the magnetic mode, the measured quantity $w(x,t)$ (transverse cantilever deflection) in the acoustic mode is the tip motion $u(t)$ relative to the base motion $y(t)$:

$$w(x,t) = u(x,t) - y(t). \quad (9)$$

Note that in Eq. (7) we consider the absolute tip motion $u(x,t)$ in an absolute, inertial reference frame, and the inertial excitation force is taken care of by the moving boundary condition. When posed in a noninertial reference frame moving with the base of the cantilever, the inertial term reappears naturally as an external driving force.

Following the same procedure as in Sec. II A, we can get the following transfer function for the ideal acoustic excitation of the i th eigenmode:

$$\begin{aligned}
\left. \frac{C_i(\omega)}{Y(\omega)} \right|_{\text{acoustic}}^{\text{ideal}} &= \frac{\omega^2 \left(\rho_c A + \frac{\pi}{4} \rho_f b^2 \Gamma_{\text{rect}} \right) \times \beta_i L}{EI(\lambda_i/L)^4 \times \alpha_i L - \omega^2 \left(\rho_c A + \frac{\pi}{4} \rho_f b^2 \Gamma_{\text{rect}} \right) \times \alpha_i L}.
\end{aligned} \quad (10)$$

For the first bending mode, $i=1$, we get

$$\begin{aligned}
\left. \frac{C_1(\omega)}{Y(\omega)} \right|_{\text{acoustic}}^{\text{ideal}} &= \frac{\omega^2 \left(\rho_c A + \frac{\pi}{4} \rho_f b^2 \Gamma_{\text{rect}} \right) \times 0.3915L}{1.0302k_c - \omega^2 \left(\rho_c A + \frac{\pi}{4} \rho_f b^2 \Gamma_{\text{rect}} \right) \times 0.25L}.
\end{aligned} \quad (11)$$

Here the input is the base amplitude $Y(\omega)$ and the output is the measured tip motion $C_1(\omega)$.

C. Brownian motion response

The governing equation for Brownian motion induced cantilever oscillation can be written as

$$EI \frac{\partial^4 w(x,t)}{\partial x^4} + \rho_c A \frac{\partial^2 w(x,t)}{\partial t^2} = f_h(w, \dot{w}) + f_B, \quad (12)$$

where f_B is the thermal fluctuating (Brownian) force. The spectral density of the Brownian force is not white and can be determined by the fluctuation-dissipation theorem²⁴

$$F_B(\omega) = 4K_B T \left(\frac{\pi}{4} \rho_f b^2 \right) \omega \times \text{img}\{\Gamma_{\text{rect}}(j\omega)\}, \quad (13)$$

where K_B is Boltzmann's constant, T is the absolute temperature, and $\text{img}\{\Gamma_{\text{rect}}(j\omega)\}$ indicates the imaginary part of the hydrodynamic function $\Gamma_{\text{rect}}(j\omega)$. The transfer function for the response of the first mode due to Brownian motion induced forcing can be shown to be

TABLE I. Properties of magnetized silicon microcantilevers and surrounding fluid

Description	Value
Cantilever length	$L=250^I/300^{II}/350^{III}$ μm
Cantilever width	$b=35$ μm
Cantilever thickness	$h=1.5-1.7$ μm
Cantilever material density	$\rho_c=2300$ kg/m^3
Cantilever Young's modulus	$E=130$ GPa
Material density of water	$\rho_f=1000$ kg/m^3
Viscosity of water	$\eta=1.0e-3$ kg/ms
Material density of air	$\rho_f=1.18$ kg/m^3
Viscosity of air	$\eta=1.86e-5$ kg/ms

$$\frac{C_1(\omega)}{TK_B} \Big|_{\text{Brownian}} = \frac{4 \left(\frac{\pi}{4} \rho_f b^2 \right) \omega \times \text{img}\{\Gamma_{\text{rect}}(j\omega)\} \times 0.3915L}{1.0302k_c - \omega^2 \left(\rho_c A + \frac{\pi}{4} \rho_f b^2 \Gamma_{\text{rect}} \right) \times 0.25L}. \quad (14)$$

Again the output is the measured tip motion $C_1(\omega)$ at a given absolute temperature T .

D. Comparison of magnetic, ideal acoustic, and Brownian transfer functions in liquids

We now compare the predictions of the transfer functions (6), (11), and (14) for specific cantilevers for which experimental data are presented later in this article. All the key parameters needed for computing these transfer functions are listed in Table I. Cantilever parameters are acquired from the manufacturer and calibrated experimentally using Sader's method.²⁵ These are low-frequency (3–10 kHz in liquids) and soft (0.1–0.3 N/m) cantilevers which are typical for imaging biological samples in liquids. Cantilevers are oscillating in de-ionized water and air at room temperature (20 °C).

The theoretically predicted transfer functions in water and air of the magnetic mode, ideal acoustic mode, and Brownian motion of cantilever II (300 μm long) are plotted in Fig. 2. In water, both the Q factor and the resonance frequencies clearly decrease compared to the case in air. Moreover, it is clear that there are major differences in water between the theoretical transfer functions of the three excitation mechanisms [Fig. 2(a)]; in contrast, these differences vanish in air [Fig. 2(b)]. The following are the major differences between the theoretical responses of the microcantilever under different excitations in liquids:

- (1) Peak-frequency response: The peak frequency of the ideal acoustic mode is actually higher than the peak frequency of Brownian motion, and the peak frequency of Brownian motion is slightly higher than the peak frequency of the magnetic mode. Note that the undamped resonance frequency of the cantilever lies between the peak frequency of the magnetic mode and the ideal acoustic mode. As the quality factor increases, the difference between these three peak frequencies decreases.

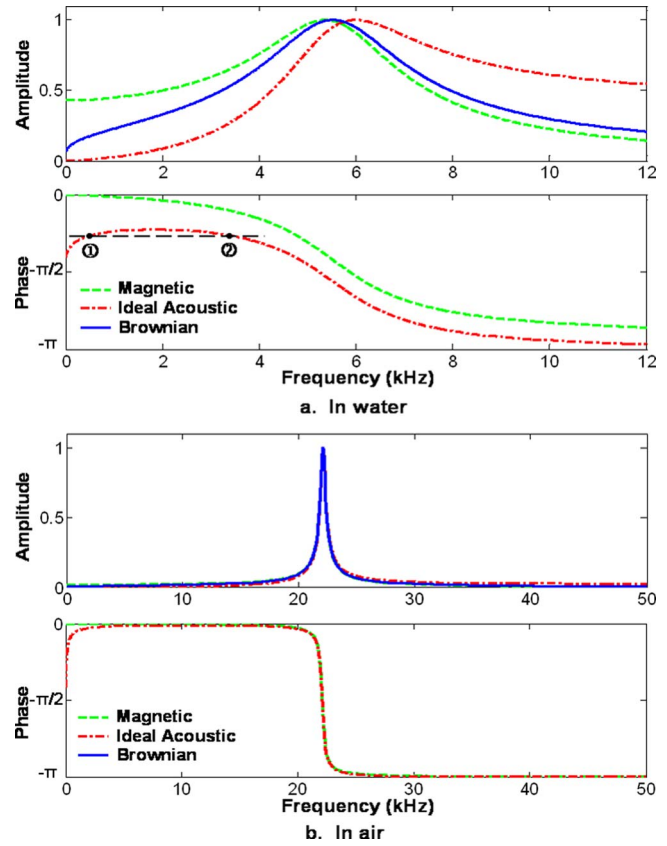


FIG. 2. (Color online) This figure shows the theoretical transfer functions of magnetic and acoustic modes and Brownian motion for cantilever II (300 μm , Table I) in (a) water and (b) in air. In water, both the Q factor and the resonance frequencies clearly decrease compared to the case in air, thus the peak frequencies of the magnetic mode, ideal acoustic mode, and Brownian motion are not the same, and the phase responses are different too. In the ideal acoustic mode one phase angle can correspond to two frequencies, for example, points ① and ②. While in air the difference between these transfer functions is nearly indistinguishable.

So in air or vacuum the difference between these three peaks (and transfer functions) is nearly indistinguishable [Fig. 2(b)]. However, as we will see from experimental data, these differences are quite significant in low- Q environments in liquids.

- (2) Observable quantity: In magnetic mode the measured quantity is the absolute motion of the tip [see $w(L, t)$ in Fig. 1(a)]. While in acoustic mode the measured quantity is not the absolute tip motion but the bending of the cantilever [see $w(L, t)$ in Fig. 1(b)]; in air this difference is negligible, but in liquids when Q factor is low the amplitude of base motion is comparable to the amplitude of tip motion.
- (3) Low and high-frequency response: At zero frequency the response amplitude of the ideal acoustic mode is zero while in magnetic mode the response amplitude is not. When the frequency is far above resonance, the response amplitude of the ideal acoustic mode will be same as the base motion (dither vibration) amplitude while in magnetic mode it goes to zero.
- (4) Phase response: In the magnetic mode the amplitude and phase characteristics are uniquely related; while in the ideal acoustic mode one phase angle can correspond to

two drive frequencies, for example, points ① and ② in Fig. 2(a) correspond to different drive frequencies but their phase is the same.

Note that the ideal acoustic mode response matches perfectly with what was measured experimentally by Jai *et al.*¹¹ by improving the cantilever holder design to remove the spurious peaks not corresponding to the resonance frequencies of the cantilever oscillation.¹⁰

E. Real acoustic mode response

The ideal acoustic mode described earlier neglects the influence of fluid-borne excitation. Now we will include this effect and aim to answer the following important questions— (a) How much does the fluid-borne excitation contribute to cantilever motion compared with the structure-borne excitation? (b) Can we quantify the fluid-borne excitation force? To answer these questions, we include the fluid-borne excitation force f_{fluid} in the governing equation

$$EI \frac{\partial^4 u(x,t)}{\partial x^4} + \rho_c A \frac{\partial^2 u(x,t)}{\partial t^2} = f_h(u, \dot{u}) + f_{\text{fluid}}(u_f, \dot{u}_f). \quad (15)$$

The fluid-borne excitation force f_{fluid} can be, in general, written in the frequency domain as^{20–22}

$$F_{\text{fluid}}(\omega) = \frac{\pi}{4} \rho_f b^2 \omega^2 \Gamma_{\text{rect}}(j\omega) U_f(\omega), \quad (16)$$

where u_f is the local flow motion generated by the vibrating cantilever chip, which strongly depends on the liquid cell geometry, the cantilever chip holder structure, and the fluid properties. $U_f(\omega)$ is the Fourier transform of u_f . It is difficult to model this local flow transient motion. However, since the fluid motion is primarily generated by the vibrating cantilever chip, we can assume that U_f is proportional to the amplitude of the cantilever chip vibration

$$U_f(\omega) = Y(\omega) \times A_{\text{fluid}}(\omega), \quad (17)$$

where $A_{\text{fluid}}(\omega)$ is the fluid drive spectrum, which is a nondimensional number. Once $A_{\text{fluid}}(\omega)$ is determined experimentally, Eqs. (16) and (17) can be used to determine the fluid-borne excitation force.

Inserting Eqs. (16) and (17) into Eq. (15), we arrive at the transfer function for the response of the microcantilever in its first eigenmode under real acoustic excitation

$$\left. \frac{C_1(\omega)}{Y(\omega)} \right|_{\text{real}} = \frac{\omega^2 \left\{ \rho_c A + \frac{\pi}{4} \rho_f b^2 \Gamma_{\text{rect}}(j\omega) \times [1 + A_{\text{fluid}}(\omega)] \right\} \times 0.3915L}{1.0302k_c - \omega^2 \left(\rho_c A + \frac{\pi}{4} \rho_f b^2 \Gamma_{\text{rect}} \right) \times 0.25L}. \quad (18)$$

By comparing the transfer function of the ideal acoustic mode Eq. (11) and real acoustic mode Eq. (18), we can calculate the response of the fluid-borne excitation as

$$\begin{aligned} \left. \frac{C_1(\omega)}{Y(\omega)} \right|_{\text{acoustic}}^{\text{fluid-borne}} &= \left. \frac{C_1(\omega)}{Y(\omega)} \right|_{\text{acoustic}}^{\text{real}} - \left. \frac{C_1(\omega)}{Y(\omega)} \right|_{\text{acoustic}}^{\text{ideal}} \\ &= \frac{\omega^2 \frac{\pi}{4} \rho_f b^2 \Gamma_{\text{rect}}(\omega) A_{\text{fluid}}(\omega) \times 0.3915L}{1.0302k_c - \omega^2 \left(\rho_c A + \frac{\pi}{4} \rho_f b^2 \Gamma_{\text{rect}} \right) \times 0.25L}. \end{aligned} \quad (19)$$

Equations (11) and (19) give the contributions to the overall cantilever response of the structure-borne excitation and the fluid-borne excitation in the acoustic mode response.

Equation (18) provides a convenient way to extract the fluid drive spectrum $A_{\text{fluid}}(\omega)$ experimentally. In Eq. (18), $C_1(\omega)$ can be measured by making frequency sweep curve, $Y(\omega)$ is \sim constant over the frequency domain and can be determined by measuring the residual vibration (vibration

after the cantilever fully contacts the sample surface), all the other parameters on the right side are known except $A_{\text{fluid}}(\omega)$. Thus we can extract $A_{\text{fluid}}(\omega)$ from a set of frequency sweep data with a known base amplitude using Eq. (18). Once $A_{\text{fluid}}(\omega)$ is obtained, we can answer our fundamental questions proposed at the beginning of this section. Moreover, the fluid-borne excitation force can be easily calculated using Eqs. (16) and (17). In what follows we describe the results of such an approach using real experimental data.

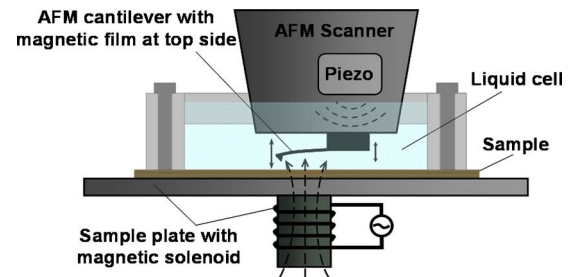


FIG. 3. (Color online) Schematic of experiment setup. A piezoelectric transducer is attached to the cantilever holder and a magnetic coil is placed at the bottom the sample plate. This system allows us to switch from acoustic mode to magnetic mode without changing any hardware or realigning the laser beam.

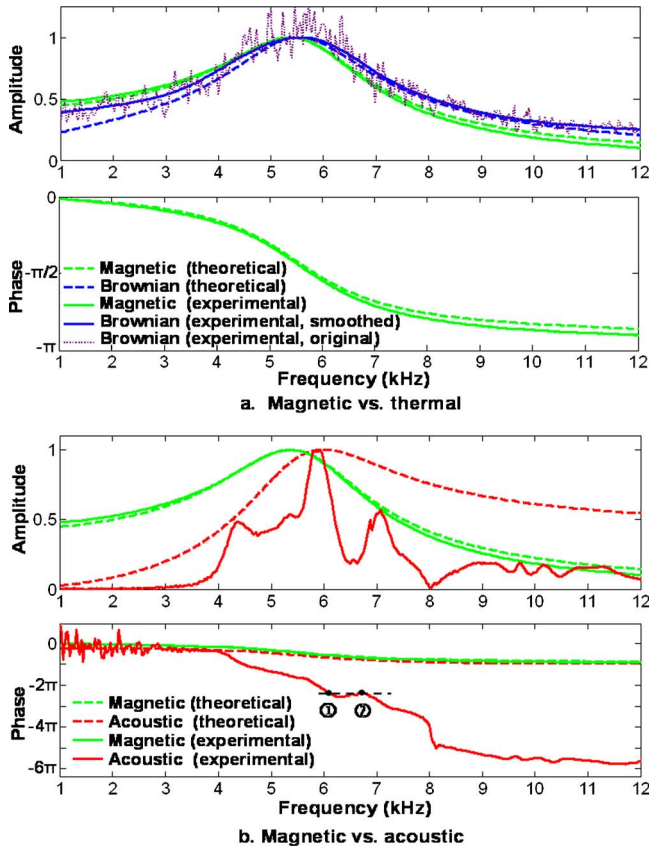


FIG. 4. (Color online) (a) A comparison of cantilever response in water with magnetic and thermal excitation and (b) a comparison of cantilever response in water with magnetic and acoustic excitation. Both experimental (solid) and theoretical (dashed) results repeated from Fig. 2(a) are plotted. All data are presented for cantilever II ($300 \mu\text{m}$ long, Table I). The theoretically predicted differences between the magnetically and thermally excited cantilever are clearly observed in experimental data. However, due to the liquid cell dynamics many artificial resonance peaks arise in the frequency sweep curve of the experimental acoustic mode.

III. EXPERIMENTAL SETTING AND FREQUENCY SWEEP CURVES

The experiment setup consists of an Agilent 5500 AFM system, an external Signal Recovery lock-in amplifier, and a data acquisition system based on National Instruments 5911 boards. Amplitude and phase data of magnetic and acoustic mode were acquired using the lock-in amplifier and the AFM control system. Thermal noise data were collected by the data acquisition system with 10^6 Hz sampling rate. The schematic of the AFM scanner and the liquid cell is shown in Fig. 3. A piezoelectric transducer is attached to the cantilever holder and a magnetic coil is placed at the bottom the sample plate. This system allows us to switch from acoustic mode to magnetic mode without changing any hardware or moving the chip, realigning the laser beam, thus ensuring a true comparison of different excitation mechanisms under identical conditions.

Experiments are performed in de-ionized water at room temperature (20°C). Five chips of magnetically coated cantilevers (Agilent Technologies), with three cantilevers (cantilever properties are listed in Table I) on each chip have been tested in this experiment. The results are all repeatable. Figure 4 shows one set of normalized frequency sweeps of

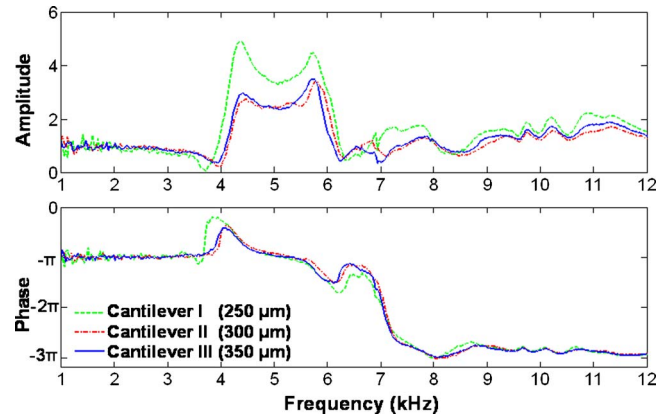


FIG. 5. (Color online) The fluid drive spectra $A_{\text{fluid}}(\omega)$ of three neighboring cantilevers (Table I) plotted using the method we described in Sec. II E.

acoustic and magnetic modes and frequency spectrum of thermal noise of cantilever II ($300 \mu\text{m}$ long) together with their corresponding theoretical curves repeated from Fig. 2(a). The plots do not show the frequency range <1 kHz because there is a high-pass (>1 kHz) filter in our system.

First we compare the magnetic mode and thermal noise spectrum in Fig. 4(a). The amplitude response of thermal noise is obtained from the square root of the power spectrum density of thermal noise (10^6 data points, 10^6 Hz sampling rate) and then smoothed using the moving-average method by MATLAB. The phase response of the thermal noise cannot be extracted by this method. As can be seen, the experimental peak frequency of thermal noise spectrum is slightly higher than that of the magnetic mode and the amplitude of magnetic mode at low frequency is not zero. The theoretically predicted transfer functions for the magnetic and thermal excitation (dashed curves) match excellently with experimental data.

In Fig. 4(b) we compare the magnetic mode with the acoustic mode response. As we have mentioned before, many artificial resonance peaks which are not related to the true dynamics of the cantilever are observed in the spectra of the real acoustic mode, making it very different from the ideal acoustic mode prediction. The phase information of the acoustic mode is also “contaminated” by these artificial resonances—one phase angle can correspond to two or more drive frequencies. In spite of these effects we can still observe some phenomena that are predicted from the theoretical transfer function analysis: the peak frequency of the acoustic mode is larger than that of the magnetic mode and the oscillation magnitude of the cantilever is nearly zero at low excitation frequencies in the acoustic mode.

We now use the method proposed in Sec. II E to extract the fluid drive spectrum $A_{\text{fluid}}(\omega)$ for the acoustically excited levers. We focus on three cantilevers which are on the same chip and next to each other. The properties of these three cantilevers are the same except their lengths are 250, 300, and $350 \mu\text{m}$, respectively (see Table I). The extracted $A_{\text{fluid}}(\omega)$ for the three cantilevers are plotted in Fig. 5. As we expect, since the experimental environments for the three cantilevers are almost the same, the resulting three $A_{\text{fluid}}(\omega)$ spectra are very similar: the peaks are at the same frequencies, only the magnitudes vary slightly.

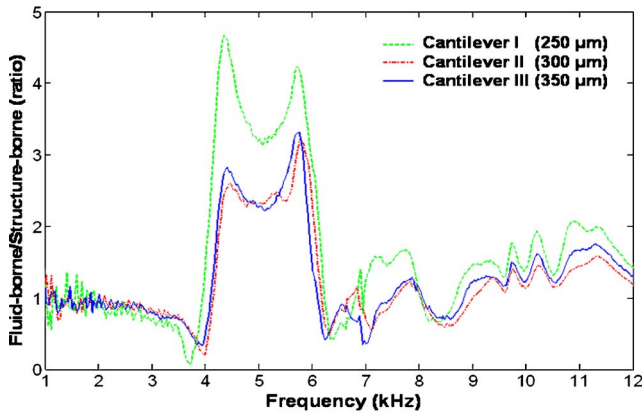


FIG. 6. (Color online) Comparison of responses of fluid-borne and structure-borne excitation for three neighboring cantilevers (Table I). The ratio of responses due to fluid-borne and fluid-borne excitation is mostly in the range of [0.5–4], and often larger than 1.

We also compare the contributions of the structure-borne and fluid-borne excitation on the three cantilevers described earlier. Figure 6 is the plot of the ratio of the right side of Eq. (19) to the right side of Eq. (11) evaluated using the method described for the three cantilevers. It is clearly seen that the ratio is mostly in the range of [0.5–4] and often larger than 1. This means that the contribution of the fluid-borne excitation is comparable to, and most of the time even greater than, the structure-borne excitation. We thus conclude that the cantilever in real acoustic mode is significantly excited by the unsteady fluid-borne excitation force in liquids.

It is interesting to compare our results with those of Schaffer *et al.*⁸ who present a different way to extract the fluid drive spectrum. According to Schaffer *et al.*, the cantilever response spectrum of acoustic mode is the product of a fluid drive spectrum, which only depends on the experimental settings, and the thermal noise spectrum, which only depends on the cantilever and fluid. It is clear from Eq. (18) that the model of Schaffer *et al.* is a special case of our more general model. Specifically, we recover Schaffer *et al.*'s model when $A_{\text{fluid}}(\omega) \gg 1$ so that the $\rho_c A$ term and $(\pi/4)\rho_f b^2 \Gamma_{\text{rect}}(j\omega) \times 1$ term in the denominator can be neglected in Eq. (18),

$$\begin{aligned} & \left. \frac{C_1(\omega)}{Y(\omega)} \right|_{\text{acoustic}}^{\text{real}} \\ &= \frac{\frac{\pi}{4}\rho_f b^2 \omega^2 \Gamma_{\text{rect}}(\omega) \times A_{\text{fluid}}(\omega) \times 0.3915L}{1.0302k_c - \omega^2 \left(\rho_c A + \frac{\pi}{4}\rho_f b^2 \Gamma_{\text{rect}}(\omega) \right) \times 0.25L} \\ &= A_{\text{fluid}}(\omega) \times \left. \frac{C_1(\omega)}{F_{\text{dr}}(\omega)} \right|_{\text{magnetic}} \times \left[\frac{\pi}{4}\rho_f b^2 \omega^2 \Gamma_{\text{rect}}(\omega) \right]. \end{aligned} \quad (20)$$

Now the cantilever response spectrum of real acoustic mode is the product of a fluid drive spectrum $A_{\text{fluid}}(\omega)$ and the magnetic mode spectrum (which is very similar to the thermal noise spectrum) scaled by the term $[\pi\rho_f b^2 \omega^2 \Gamma_{\text{rect}}(\omega)/4]$. This implies that Schaffer *et al.*'s model assumes implicitly

that the structure-borne excitation is negligible. We have already seen in this work that although the structure-borne excitation is smaller than the fluid-borne vibration, it is by no means negligible.

IV. IMPLICATIONS AND CONCLUSIONS

The results presented earlier bear significant implications for amplitude and frequency modulated AFM in liquid environments:

- (1) In the magnetic mode, the cantilever responds significantly even at low drive frequencies. In fact, since the Q factor in liquid is quite low, the response magnitude at low frequency is comparable to the peak magnitude. This implies that the magnetic mode can be operated at frequency lower than the peak frequency. In fact Schindler *et al.* have pointed out that the best sensitivity for molecular recognition magnetic mode AFM is always obtained at the left side of the resonance.²⁶
- (2) In the acoustic mode the measured quantity is not the absolute tip motion but the bending of the cantilever (i.e., the relative tip motion to the base motion). In low Q -factor systems the amplitude of base motion is comparable to the amplitude of absolute tip motion, making the measured quantity very different from the absolute tip motion.
- (3) For the acoustic mode in liquids, it is essential to locate the resonance frequency of the cantilever which sometimes could be submerged in the “forest of peaks.”⁸ From our results we know that the peak frequency of the ideal acoustic ω_{acous} is larger than the undamped resonance frequency ω_0 while the peak frequency of the magnetic mode ω_{mag} or the peak frequency of the spectra of thermal noise ω_{thermal} is smaller than ω_0 . Thus while using acoustically excited AFM, one should choose a drive frequency which is close to but slightly greater than ω_{thermal} (or ω_{mag}). So long as we can identify the resonance peak of the cantilever, we can use amplitude modulation AFM (AM-AFM) by acoustically excited the cantilever.
- (4) For frequency modulation AFM (FM-AFM), both well-defined resonance peak and phase signal are essential. This is no problem with the magnetic mode²⁷ because both amplitude and phase responses are very clear [Fig. 4(a)]. But for the acoustic mode, one phase angle can correspond to two or more frequencies due to the artificial resonance peaks, for example, points ① and ② in Fig. 4(b) have the same phase and their drive frequencies are very close. Clearly, if the operating phase is not chosen correctly, then the working frequency could jump from one drive frequency to another leading to unstable scanning.
- (5) Recently, extensive efforts have been made to estimate the tip-sample interaction force and energy dissipation^{28,29} in dynamic AFM in air. However, these results cannot directly be applied to acoustically driven cantilevers in liquids because the assumed relationship $A_0 = QA_d$ between the drive amplitude A_d and free oscillation amplitude A_0 is no longer valid due to low Q

factors and the significant presence of fluid-borne excitation force. In principle, with accurate knowledge of transfer functions and of the fluid-borne forces as outlined in this article, it becomes possible to measure tip-sample energy dissipation in liquids using acoustic excitation.

In summary, the theoretical and experimental differences between the response of AFM microcantilevers in liquids to magnetic, acoustic, and thermal (Brownian motion induced) excitations have been clearly outlined. Some differences are subtle such as those between thermal excitation and magnetic excitation, while others are large such as for ideal and real acoustic modes. A method has been proposed to estimate quantitatively the unsteady structure-borne and fluid-borne excitation forces acting on the acoustically excited AFM cantilever. The results have significant implications both for amplitude and frequency modulated AFM operation in liquids.

ACKNOWLEDGMENTS

The authors acknowledge financial support from the NSF through the Grant No. CMS-0409660. The authors also thank Professor P. J. de Pablo and C. Carrasco (Universidad Autonoma de Madrid, Spain) for useful discussions.

- ¹F. Moreno-Herrero, J. Colchero, J. Gomez-Herrero, and A. M. Baro, *Phys. Rev. E* **69**, 031915 (2004).
- ²F. Kienberger, C. Rankl, V. Pastushenko, R. Zhu, D. Blaas, and P. Hinterdorfer, *Structure* **13**, 1247 (2005).
- ³C. A. J. Putman, K. O. Van der Werf, B. G. De Groot, N. F. Van Hulst, and J. Greve, *Appl. Phys. Lett.* **64**, 2454 (1994).
- ⁴W. Han and S. M. Lindsay, *Appl. Phys. Lett.* **69**, 4111 (1996).
- ⁵B. Rogers, D. York, N. Whisman, M. Jones, K. Murray, and J. D. Adams, *Rev. Sci. Instrum.* **73**, 3242 (2002).
- ⁶J. Tamayo, A. D. L. Humphris, and M. J. Miles, *Appl. Phys. Lett.* **77**, 582 (2000).

- ⁷A. Buguin, O. Du Roure, and P. Silberzan, *Appl. Phys. Lett.* **78**, 2982 (2001).
- ⁸T. E. Schaffer, J. P. Cleveland, F. Ohnesorge, D. A. Walters, and P. K. Hansma, *J. Appl. Phys.* **80**, 3622 (1996).
- ⁹I. Revenko and R. Proksch, *J. Appl. Phys.* **87**, 526 (2000).
- ¹⁰A. Maali, C. Hurth, T. Cohen-Bouhacina, G. Couturier, and J. P. Aime, *Appl. Phys. Lett.* **88**, 163504 (2006).
- ¹¹C. Jai, T. Cohen-Bouhacina, and A. Maali, *Appl. Phys. Lett.* **90**, 113512 (2007).
- ¹²T. Fukuma, M. Kimura, K. Kobayashi, K. Matsushige, and H. Yamada, *Rev. Sci. Instrum.* **76**, 053704 (2005).
- ¹³D. Ebeling, H. Holscher, and B. Anczykowski, *Appl. Phys. Lett.* **89**, 203511 (2006).
- ¹⁴S. P. Jarvis, A. Oral, T. P. Weihs, and J. B. Pethica, *Rev. Sci. Instrum.* **64**, 3515 (1993).
- ¹⁵E.-L. Florin, M. Radmacher, B. Fleck, and H. E. Gaub, *Rev. Sci. Instrum.* **65**, 639 (1994).
- ¹⁶S. P. Jarvis, H. Yamada, S.-I. Yamamoto, and H. Tokumoto, *Rev. Sci. Instrum.* **67**, 2281 (1996).
- ¹⁷A. Gannepalli, A. Sebastian, J. Cleveland, and M. Salapaka, *Appl. Phys. Lett.* **87**, 111901 (2005).
- ¹⁸G. C. Ratcliff, D. A. Erie, and R. Superfine, *Appl. Phys. Lett.* **72**, 1911 (1998).
- ¹⁹F. J. Rubio-Sierra, R. Vazquez, and R. W. Stark, *IEEE Trans. NanoTechnol.* **5**, 692 (2006).
- ²⁰E. O. Tuck, *J. Eng. Math.* **3**, 29 (1969).
- ²¹J. E. Sader, *J. Appl. Phys.* **84**, 64 (1998).
- ²²C. P. Green and J. E. Sader, *Phys. Fluids* **17**, 073102 (2005).
- ²³R. D. Blevins, *Formulas for Natural Frequency and Mode Shape*, 2nd ed. (Krieger, Florida, 1995).
- ²⁴M. R. Paul and M. C. Cross, *Phys. Rev. Lett.* **92**, 235501 (2004).
- ²⁵J. E. Sader, J. W. M. Chon, and P. Mulvaney, *Rev. Sci. Instrum.* **70**, 3967 (1999).
- ²⁶H. Schindler, D. Badt, P. Hunterdorfer, F. Keinberger, A. Raab, S. Wielert, and V. Ph. Pastushenko, *Ultramicroscopy* **82**, 227 (2000).
- ²⁷M. J. Higgins, C. K. Riener, T. Uchihashi, J. E. Sader, R. McKendry, and S. P. Jarvis, *Nanotechnology* **16**, S85 (2005).
- ²⁸B. Anczykowski, B. Gotsmann, H. Fuchs, J. P. Cleveland, and V. B. Elings, *Appl. Surf. Sci.* **140**, 376 (1999).
- ²⁹R. Garcia, C. J. Gomez, N. F. Martinez, S. Patil, C. Dietz, and R. Magerle, *Phys. Rev. Lett.* **97**, 016103 (2006).